US009372256B2

(12) **United States Patent**
Mohamadi

(10) **Patent No.: US 9,372,256 B2**
(45) **Date of Patent: Jun. 21, 2016**

(54) **WAFER SCALE SENSOR ULTRA-WIDEBAND ARRAY FOR TISSUE DIAGNOSIS**

(71) Applicant: **Farrokh Mohamadi**, Irvine, CA (US)

(72) Inventor: **Farrokh Mohamadi**, Irvine, CA (US)

(73) Assignee: **Farrokh Mohamadi**, Irvine, CA (US)

(*) Notice: Subject to any disclaimer, the term of this patent is extended or adjusted under 35 U.S.C. 154(b) by 340 days.

(21) Appl. No.: **14/191,118**

(22) Filed: **Feb. 26, 2014**

(65) **Prior Publication Data**

US 2015/0241552 A1 Aug. 27, 2015

(51) **Int. Cl.**

G01S 7/02	(2006.01)
G01S 13/02	(2006.01)
G01S 13/88	(2006.01)
G01S 13/89	(2006.01)
A61B 5/05	(2006.01)
H01Q 9/40	(2006.01)
H01Q 9/42	(2006.01)

(Continued)

(52) **U.S. Cl.**

CPC ***G01S 7/02*** (2013.01); ***A61B 5/0507*** (2013.01); ***A61B 5/4312*** (2013.01); ***A61B 5/7225*** (2013.01); ***G01S 7/026*** (2013.01); ***G01S 13/0209*** (2013.01); ***G01S 13/89*** (2013.01); ***H01Q 9/40*** (2013.01); ***H01Q 9/42*** (2013.01); ***H01Q 21/061*** (2013.01); *A61B 2562/046* (2013.01); *G01S 13/88* (2013.01); *G01S 13/887* (2013.01)

(58) **Field of Classification Search**

CPC G01S 7/024; G01S 7/026; G01S 13/0209; G01S 13/88; G01S 13/887; G01S 13/888; G01S 13/89; H01Q 21/061; A61B 5/05; A61B 5/0507; A61B 5/4312; A61B 5/7225; A61B 2562/046

USPC 342/22, 188

See application file for complete search history.

(56) **References Cited**

U.S. PATENT DOCUMENTS

4,630,051 A * 12/1986 Adams G01S 15/8979 342/133

4,717,916 A * 1/1988 Adams G01S 13/4454 342/107

(Continued)

OTHER PUBLICATIONS

Zhang, et al., "Multi-objective Experiment Using Ultrashort-Pulse Radar System for Breast Cancer Detection", Art, Science and Technology Center for Cooperative Research, Kyushu University, Japan, pp. 1-2.

(Continued)

Primary Examiner — Peter Bythrow

(74) *Attorney, Agent, or Firm* — Haynes and Boone, LLP

(57) **ABSTRACT**

Radar imaging for medical diagnosis addresses the need for non-ionizing and low-cost alternatives to conventional medical diagnosis methods, such as mammography x-ray techniques, which expose patients to ionizing radiation for cancer detection. An ultra wide band (UWB) sensor can produce very fine beams at the V- or W-bands using beam forming techniques developed specifically for wafer scale antenna arrays. The high bandwidth radio waves can penetrate tissue and resolve tissue anomalies with high-resolution. Pseudo-random coding creates a signal that allows the correlating receiver to extract very low energy reflected signals from background noise providing coding gain. An integrated panel of sensor antenna arrays enables rapid scanning of the subject area, such as breast tissue, to detect anomalies by eliminating the need for mechanical scanning (e.g., moving the sensors relative to the subject) because the wafer scale antenna array can instantaneously take the desired topographic picture of the subject area.

19 Claims, 14 Drawing Sheets

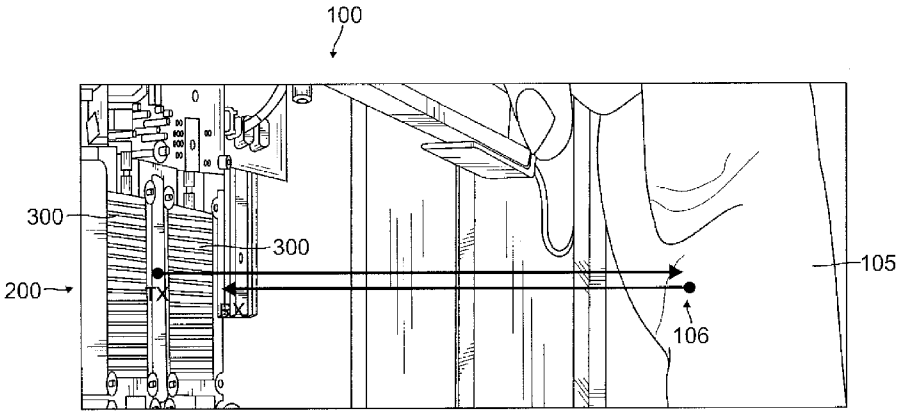

(51) **Int. Cl.**
H01Q 21/06 (2006.01)
A61B 5/00 (2006.01)

(56) **References Cited**

U.S. PATENT DOCUMENTS

5,920,285	A *	7/1999	Benjamin	G01S 13/89 342/22
6,396,450	B1 *	5/2002	Gilbert	H01J 29/10 342/374
6,777,684	B1 *	8/2004	Volkov	G01N 21/3581 250/341.1
6,967,612	B1 *	11/2005	Gorman	G01S 7/412 342/175
7,081,850	B2 *	7/2006	Small	G01S 7/282 342/134
7,791,556	B2 *	9/2010	Mohamadi	H01P 1/184 343/795
7,830,989	B2 *	11/2010	Mohamadi	G01S 7/032 343/850
7,839,283	B2	11/2010	Mohamadi	
7,855,695	B2 *	12/2010	Mohamadi	H01L 23/66 343/700 MS
7,884,757	B2 *	2/2011	Mohamadi	G01S 7/2926 342/118
7,884,776	B2 *	2/2011	Mohamadi	H01L 23/66 343/850
8,077,072	B2	12/2011	Mohamadi et al.	
8,154,339	B2 *	4/2012	Zolghadri	H01P 5/12 330/124 R
8,237,604	B2 *	8/2012	Mohamadi	G01S 7/032 342/200
8,330,642	B2 *	12/2012	Jin	G01S 13/9035 342/159
8,358,234	B2	1/2013	Mohamadi et al.	
9,285,461	B2 *	3/2016	Swirhun	G01S 7/026
2005/0270231	A1 *	12/2005	Small	G01S 7/252 342/194
2009/0224964	A1 *	9/2009	Raney	G01S 7/026 342/25 F
2010/0060509	A1 *	3/2010	Chambers	G01S 7/411 342/22
2010/0214150	A1 *	8/2010	Lovberg	G01K 11/0066 342/22
2010/0225520	A1 *	9/2010	Mohamadi	G01S 7/032 342/21
2011/0040176	A1 *	2/2011	Razansky	A61B 5/0095 600/425
2011/0298680	A1 *	12/2011	Shylo	A61B 5/015 343/762
2012/0001674	A1 *	1/2012	Mohamadi	H01P 5/12 327/355
2012/0019406	A1 *	1/2012	Sarkis	A61B 5/0507 342/22
2013/0307716	A1 *	11/2013	Mohamadi	G01S 13/887 342/22
2014/0266866	A1 *	9/2014	Swirhun	G01S 7/026 342/188

OTHER PUBLICATIONS

Chahat, et al., "New Method for Determining Dielectric Properties of Skin and Phantoms at Millimeter Waves Based on Heating Kinetics", IEEE Transactions on Microwave Theory and Techniques, vol. 60, No. 3, pp. 827-831, Mar. 2012.

Ocket, et al., "Dielectric Characterization of Biological Liquids and Tissues up to 110 GHz using an LTCC CPW Sensor", IEEE, BioWireleSS, pp. 43-45, 2013.

* cited by examiner

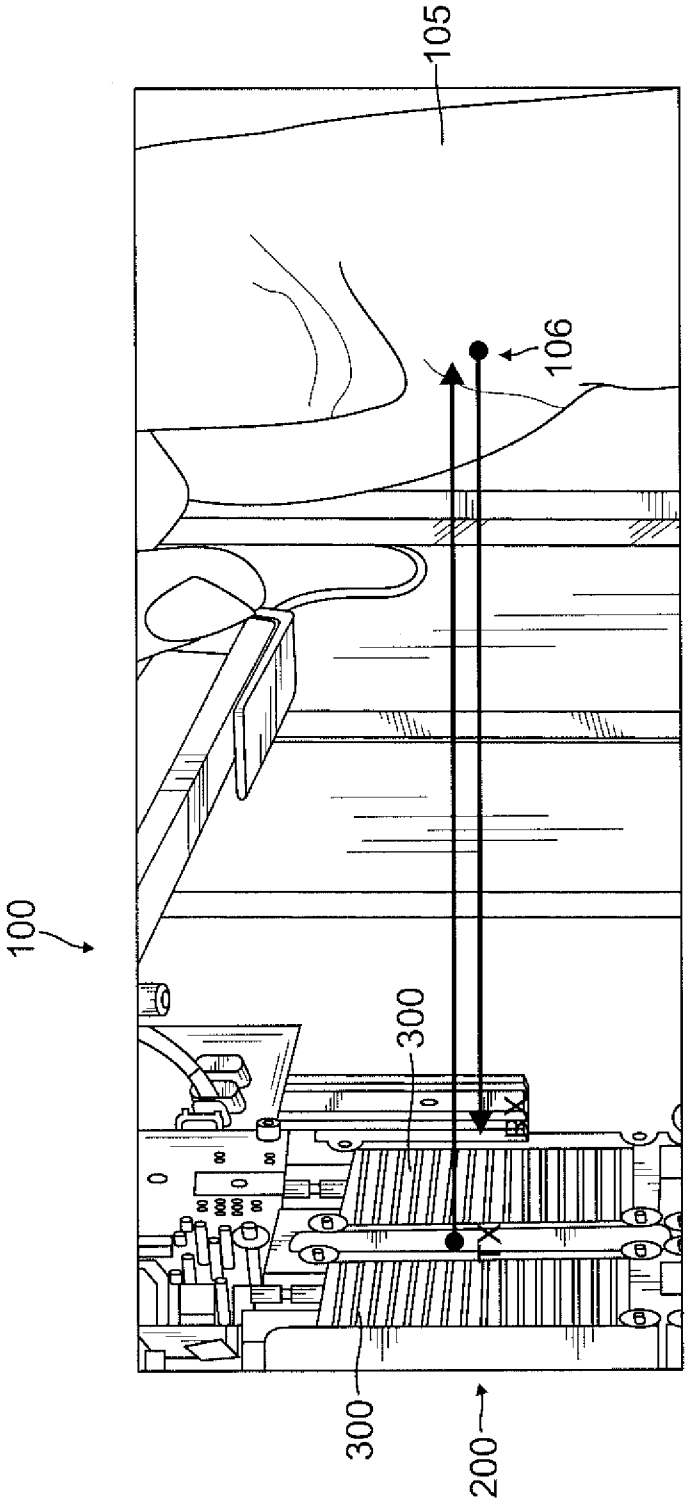

FIG. 1

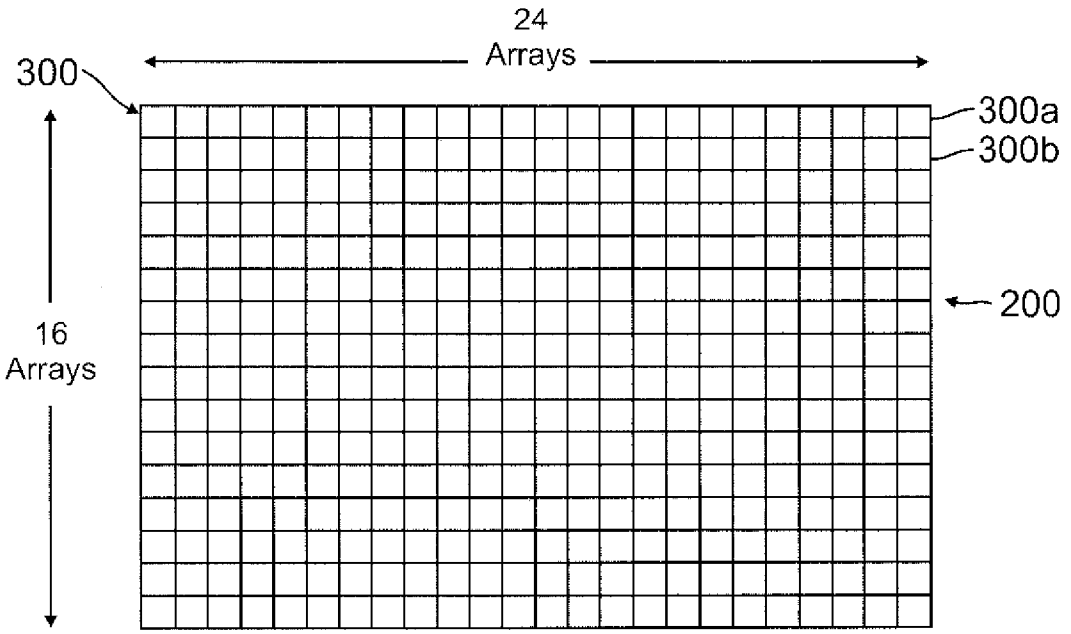

FIG. 2A

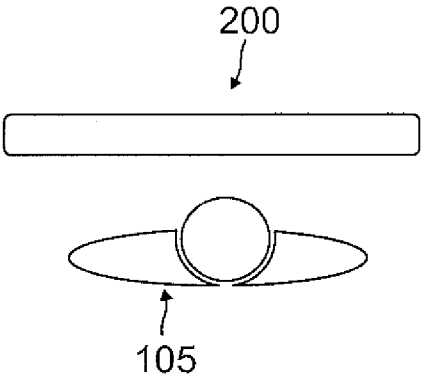

FIG. 2B

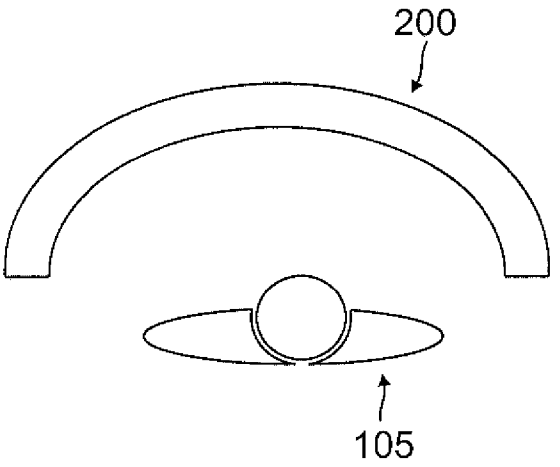

FIG. 2C

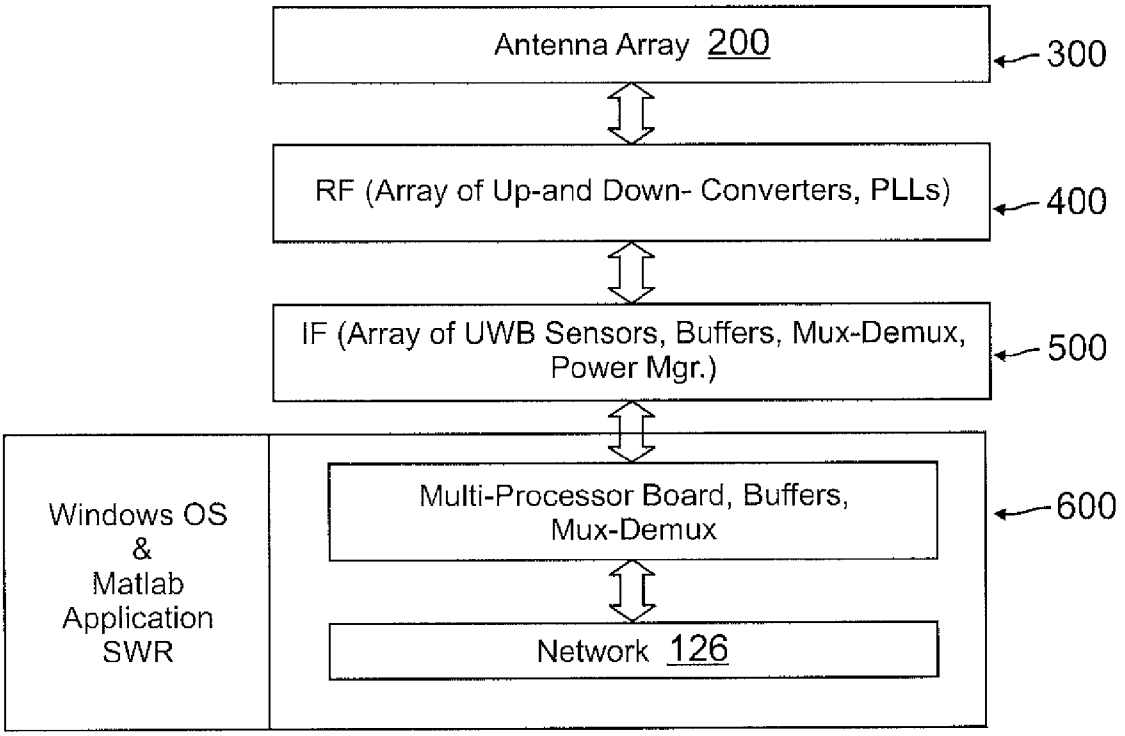
Antenna Array 200
300
RF (Array of Up-and Down- Converters, PLLs)
400
IF (Array of UWB Sensors, Buffers, Mux-Demux, Power Mgr.)
500
Windows OS & Matlab Application SWR
Multi-Processor Board, Buffers, Mux-Demux
600
Network 126

FIG. 3A

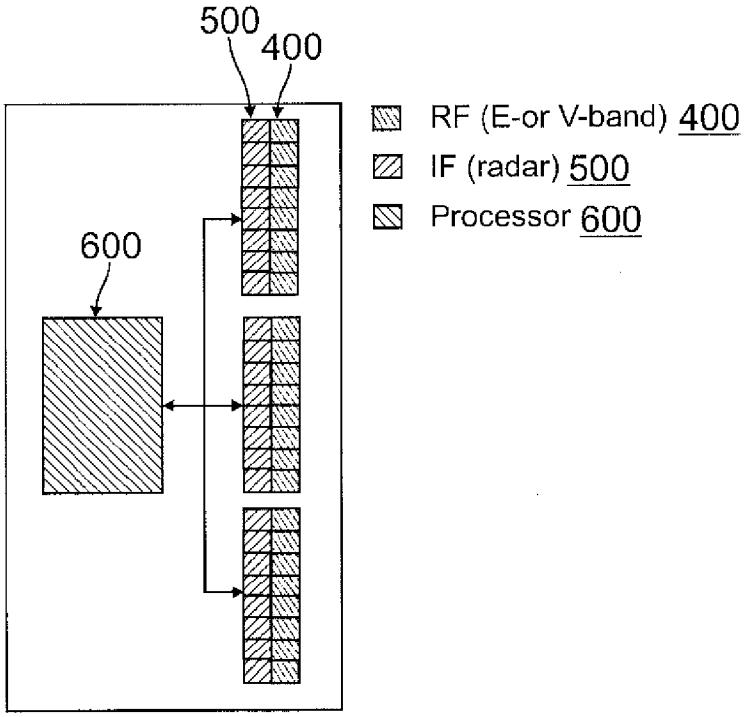
500
400
600
RF (E-or V-band) 400
IF (radar) 500
Processor 600

FIG. 3B

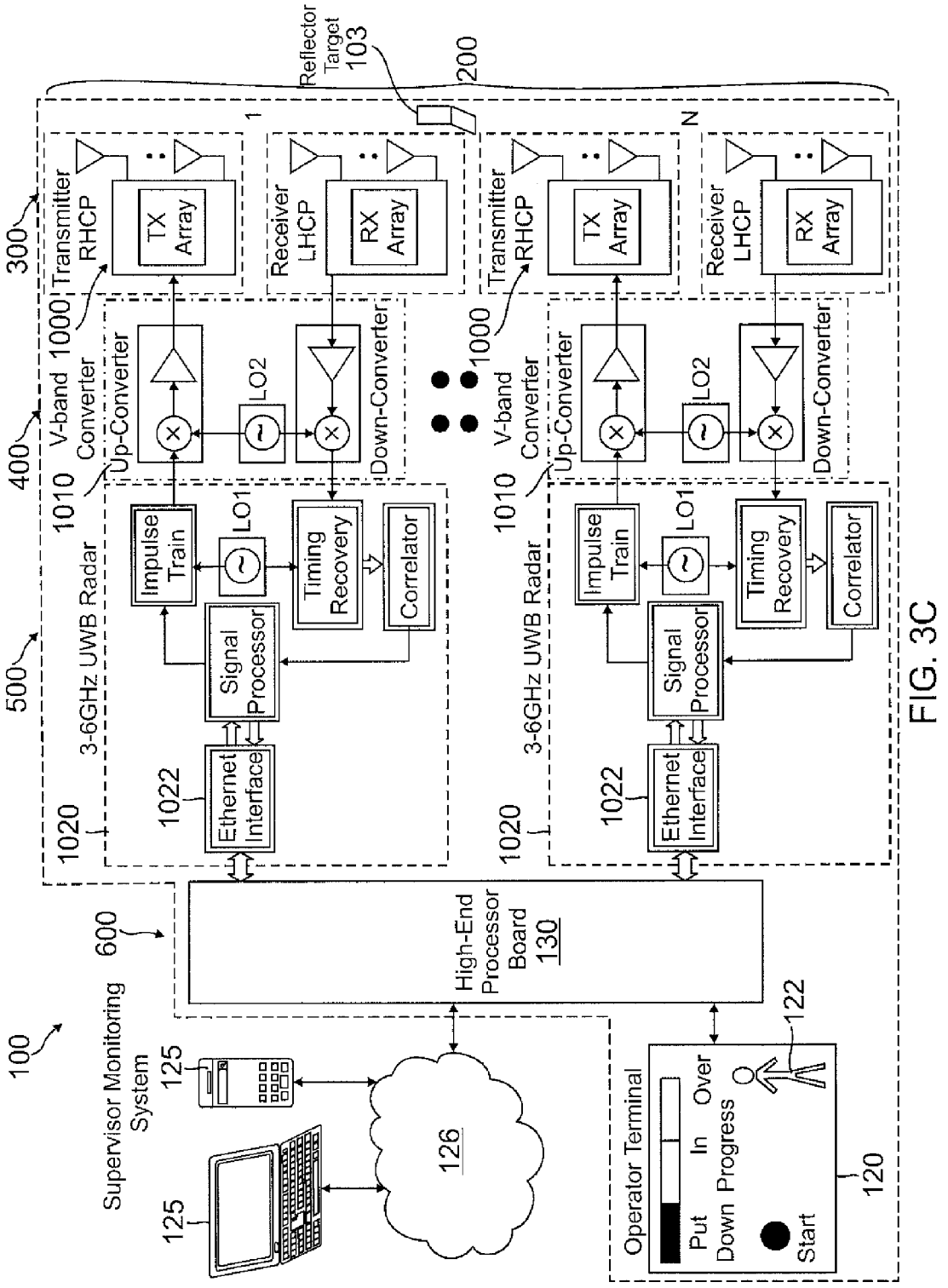
100
Supervisor Monitoring System
125
125
126
600
High-End Processor Board 130
500
3-6GHz UWB Radar
1020
1022
Ethernet Interface
Signal Processor
Impulse Train
LO1
Timing Recovery
Correlator
400
V-band Converter
1010
Up-Converter
Down-Converter
LO2
1000
300
Transmitter RHCP
Receiver LHCP
TX Array
RX Array
1
N
Reflector Target 103
200
Operator Terminal
Put Down
In Progress
Over
Start
120
122

FIG. 3C

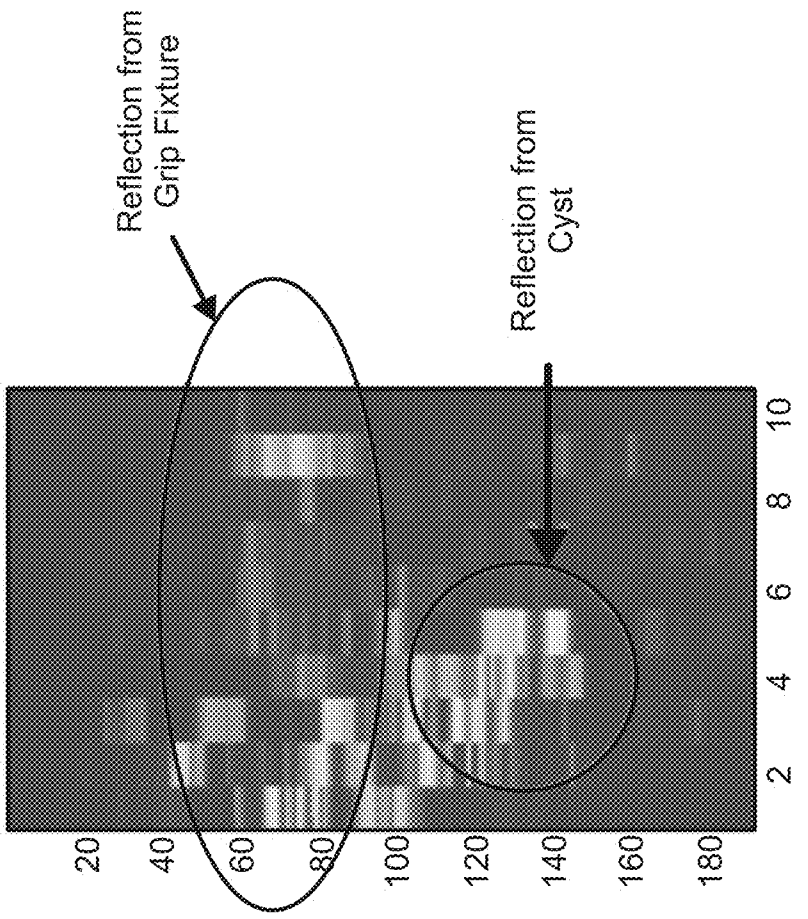
Reflection from Grip Fixture
Reflection from Cyst
20
40
60
80
100
120
140
160
180
2
4
6
8
10

FIG. 4B

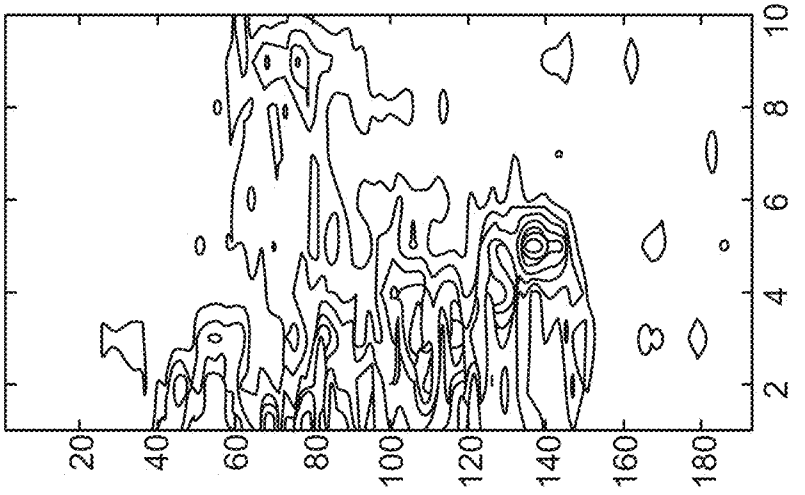
20
40
60
80
100
120
140
160
180
2
4
6
8
10

FIG. 4A

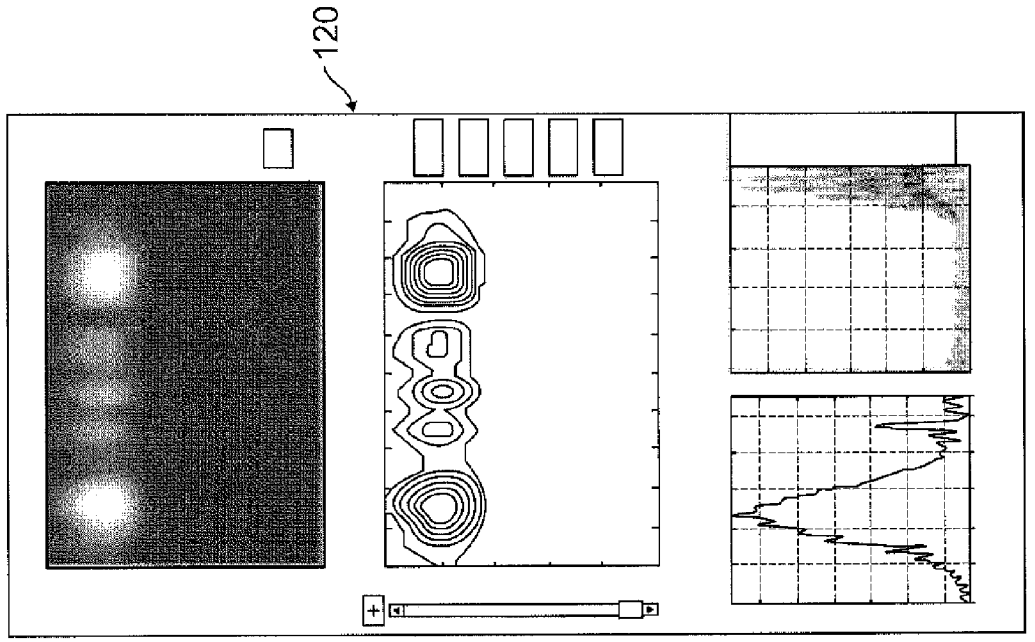
120

FIG. 5B

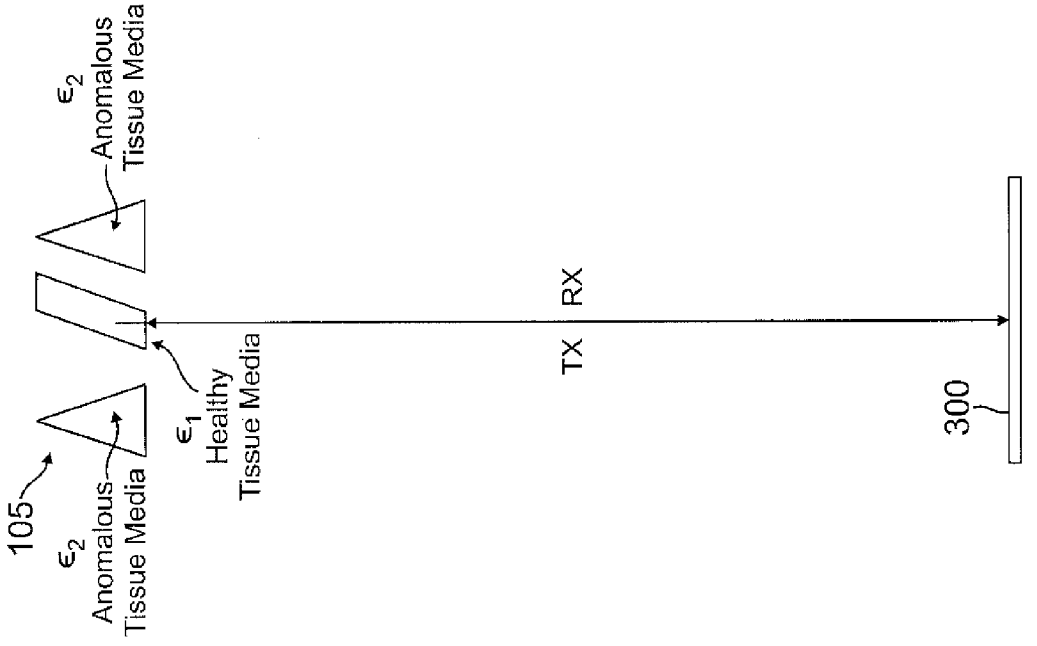
105
ϵ_2
Anomalous
Tissue Media
ϵ_1
Healthy
Tissue Media
ϵ_2
Anomalous
Tissue Media
TX
RX
300

FIG. 5A

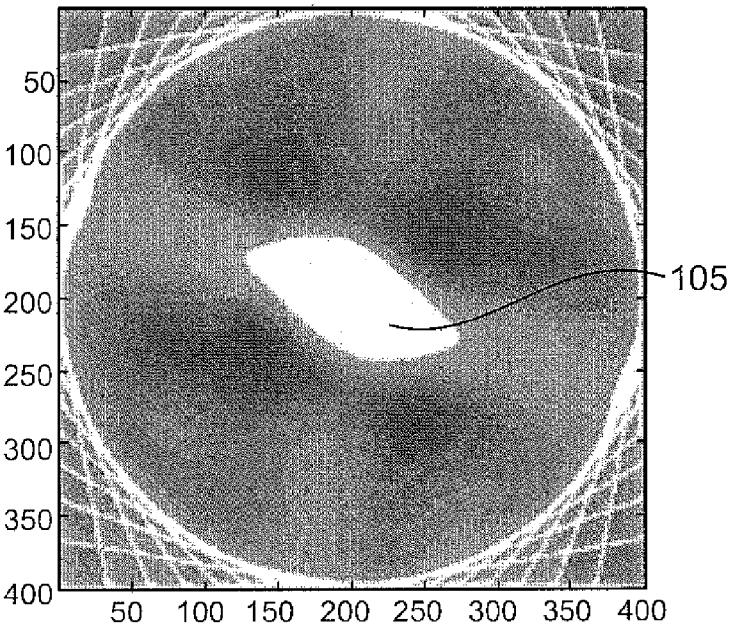
50
100
150
200
250
300
350
400
50 100 150 200 250 300 350 400
105

FIG. 6A

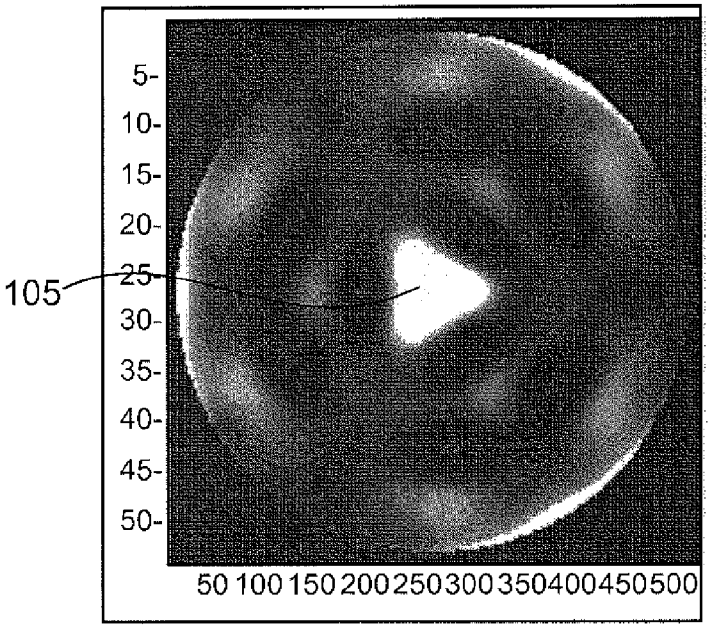
5-
10-
15-
20-
25-
30-
35-
40-
45-
50-
50 100 150 200 250 300 350 400 450 500
105

FIG. 6B

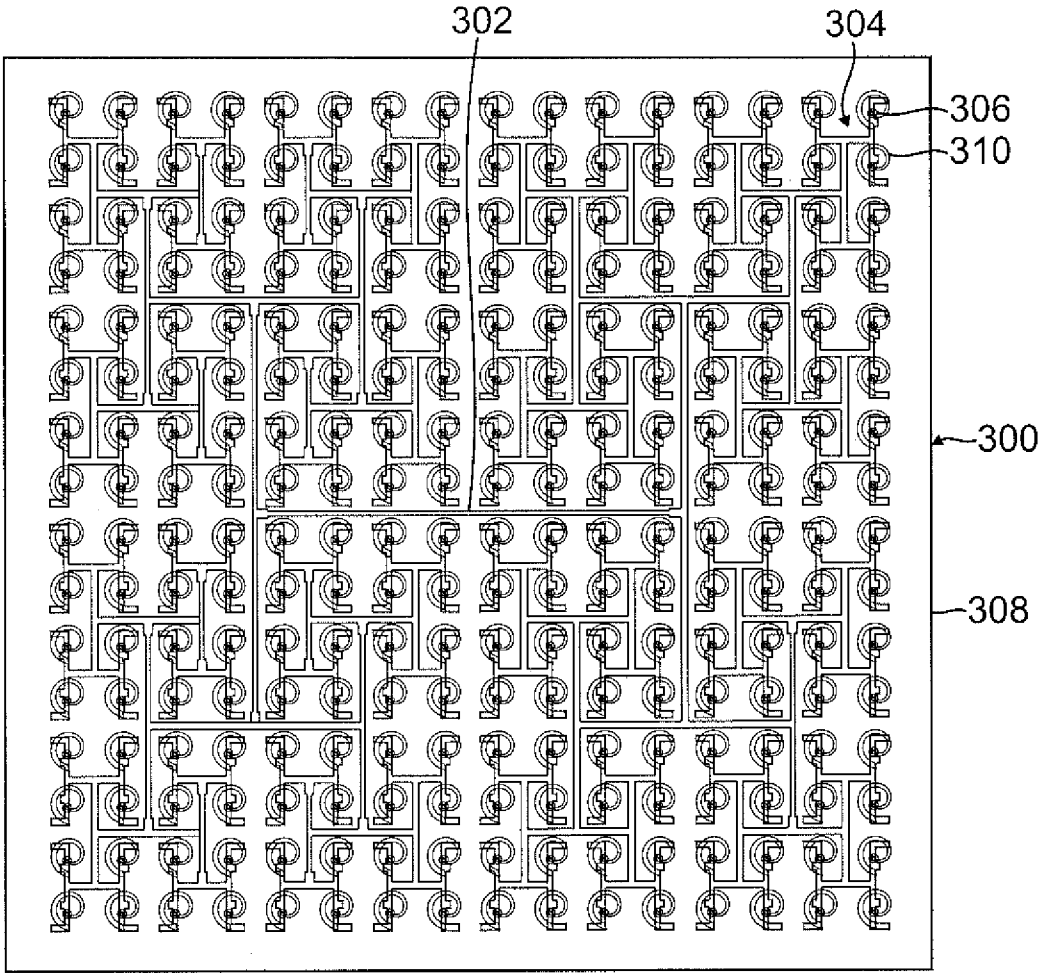

FIG. 7

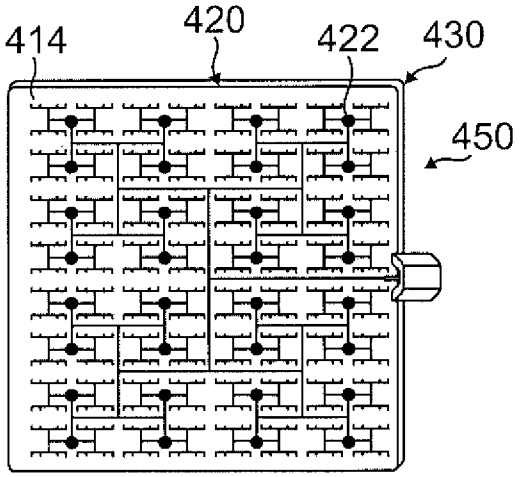

FIG. 8

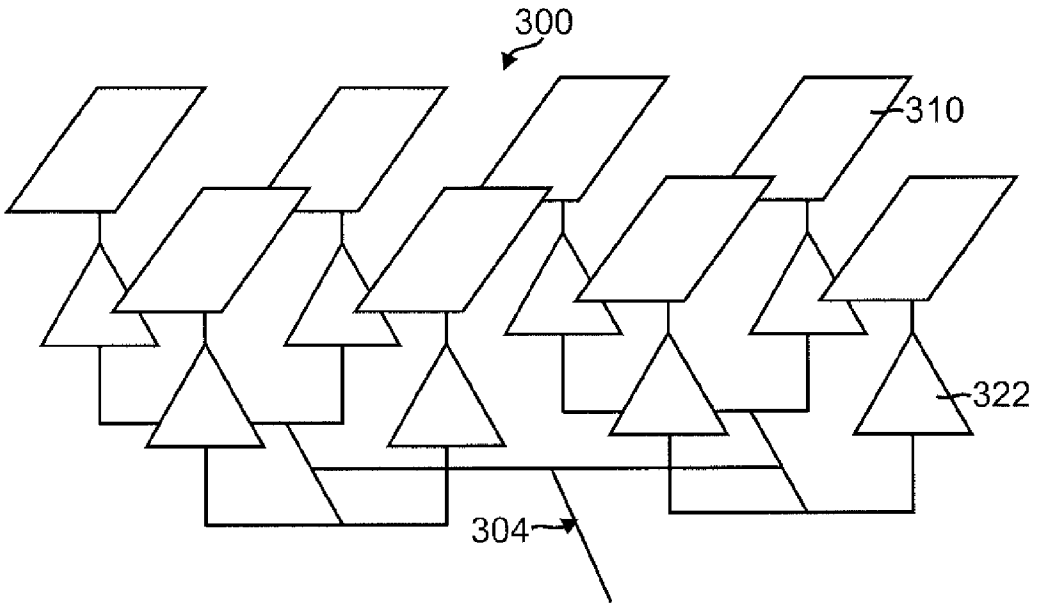

FIG. 9A

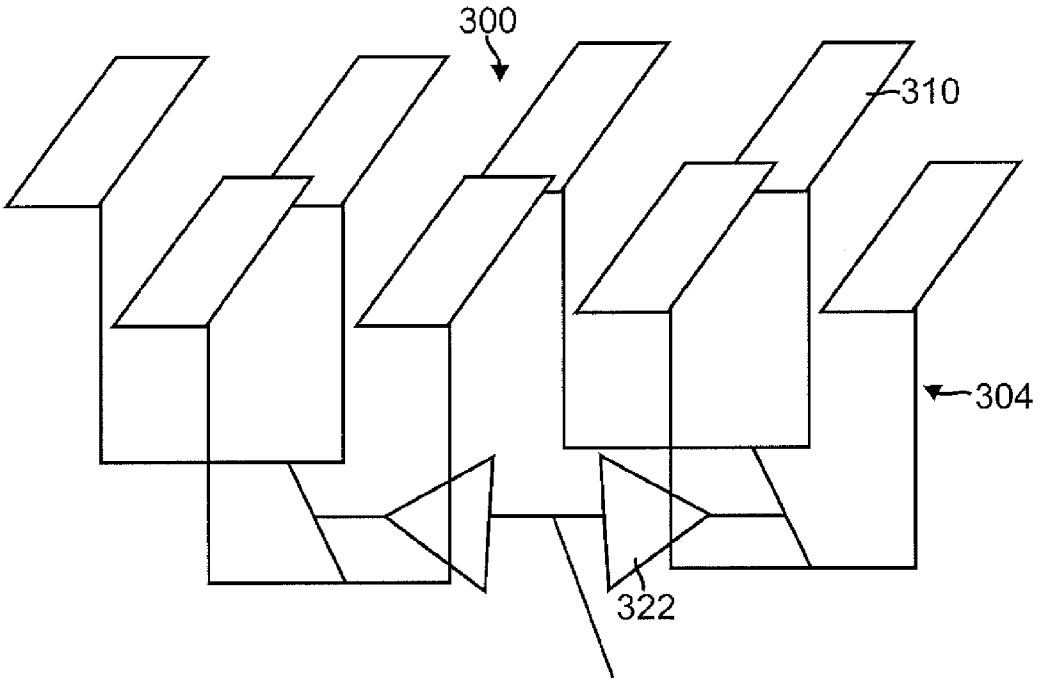

FIG. 9B

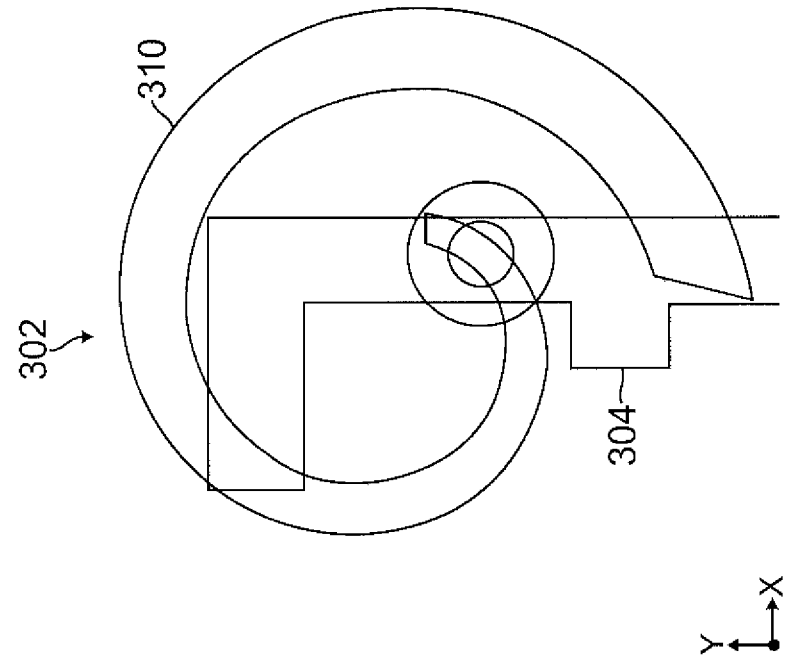

FIG. 10B

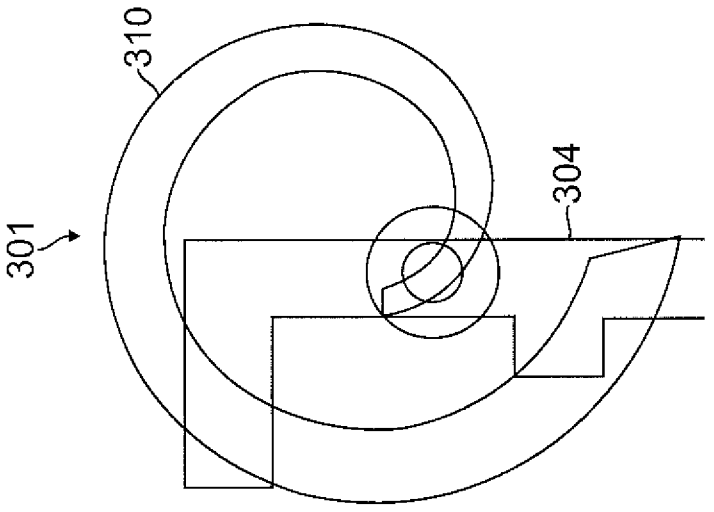

FIG. 10A

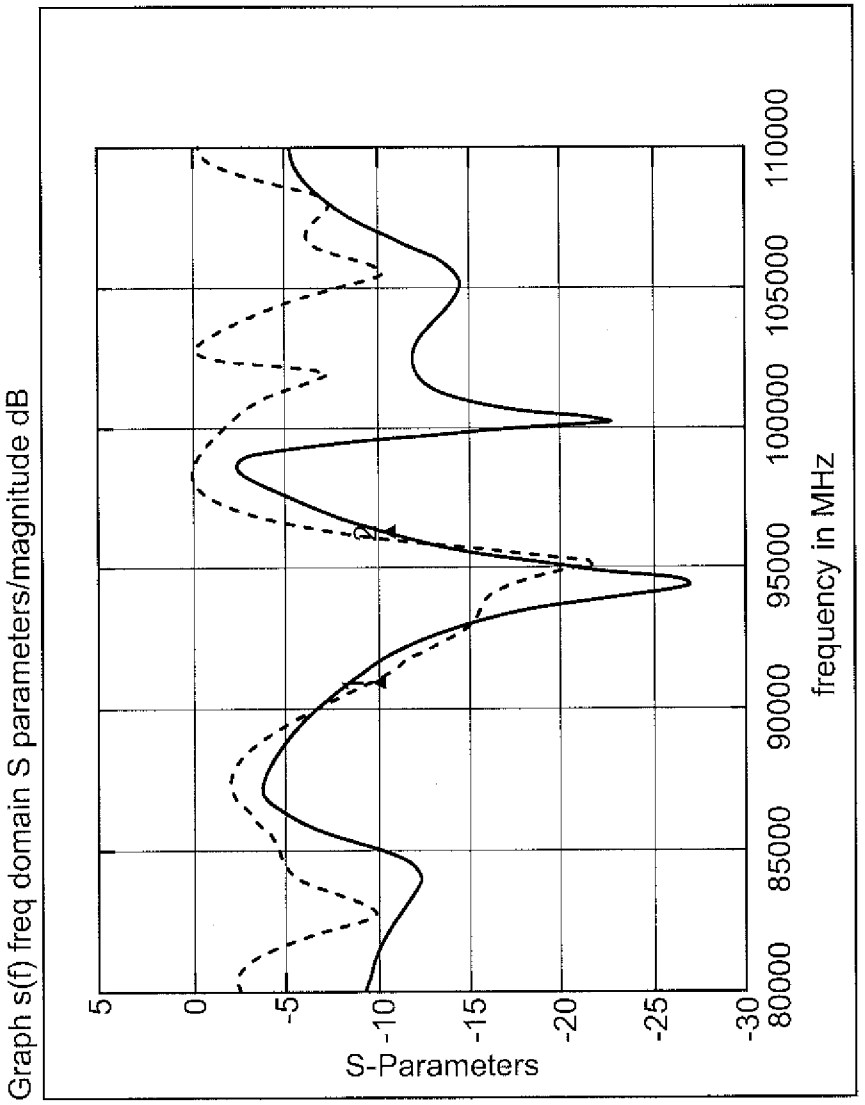
Graph s(f) freq domain S parameters/magnitude dB
S-Parameters
5
0
-5
-10
-15
-20
-25
-30
80000
85000
90000
95000
100000
105000
110000
frequency in MHz

FIG. 11

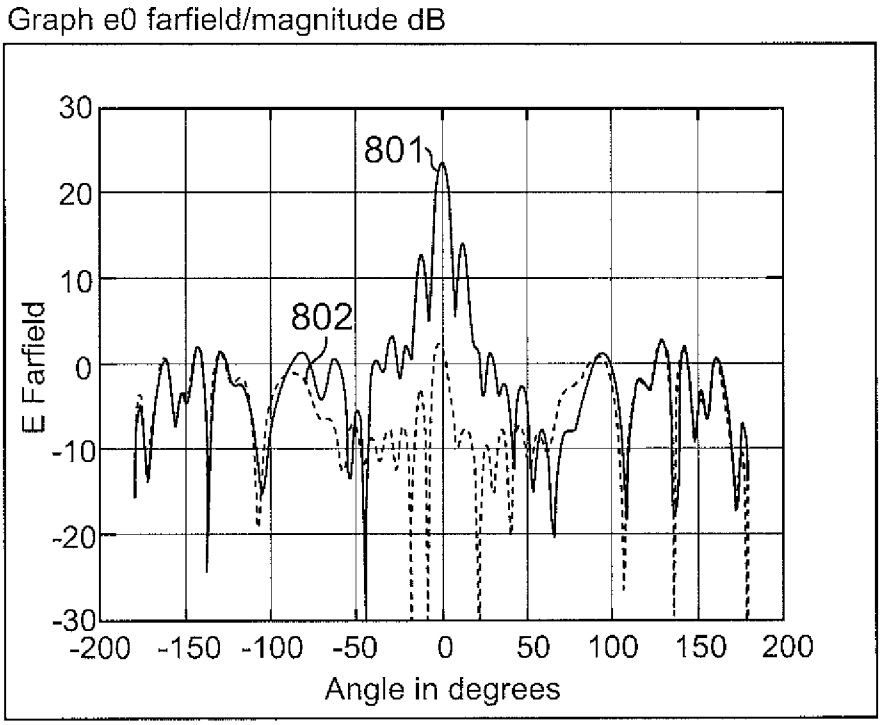

FIG. 12A

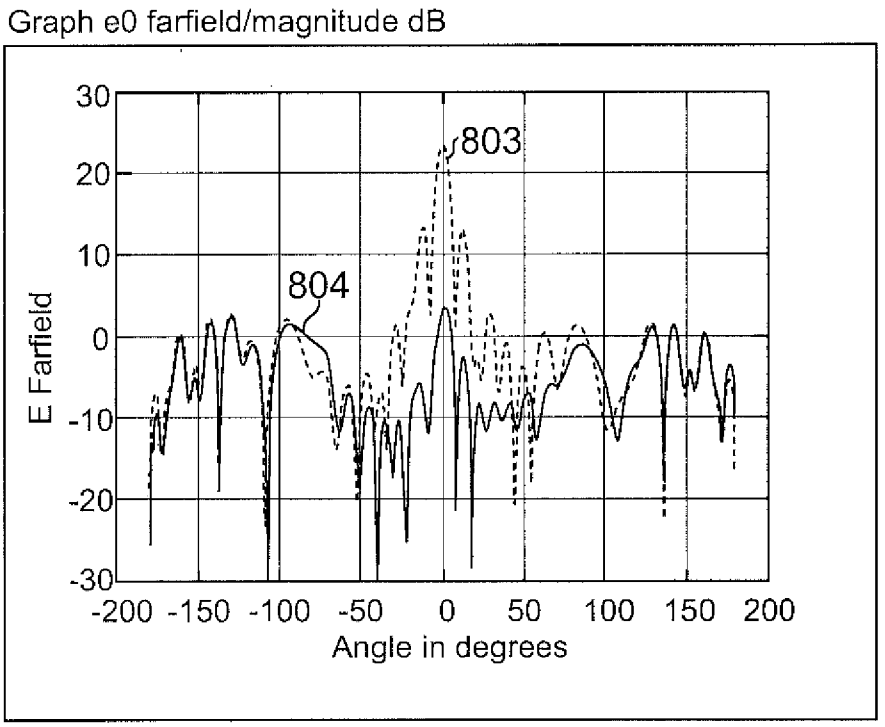

FIG. 12B

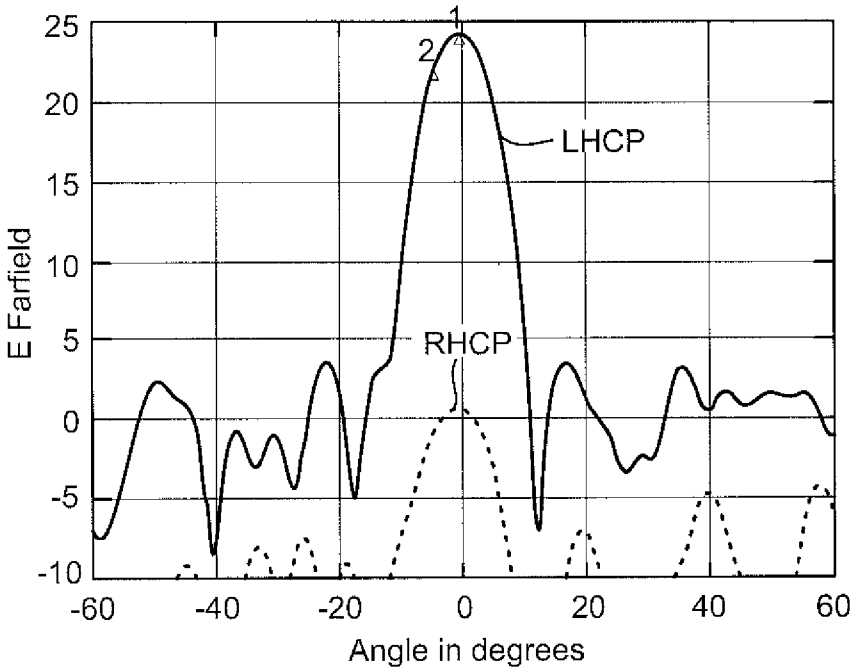

FIG. 13

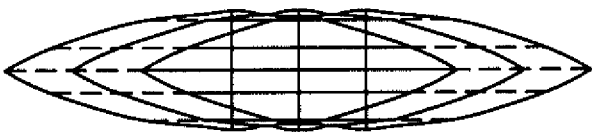

FIG. 14A

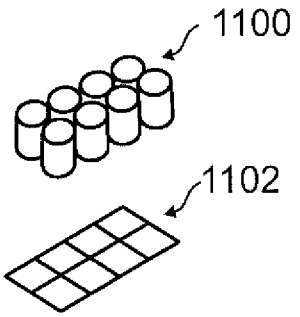

FIG. 14B

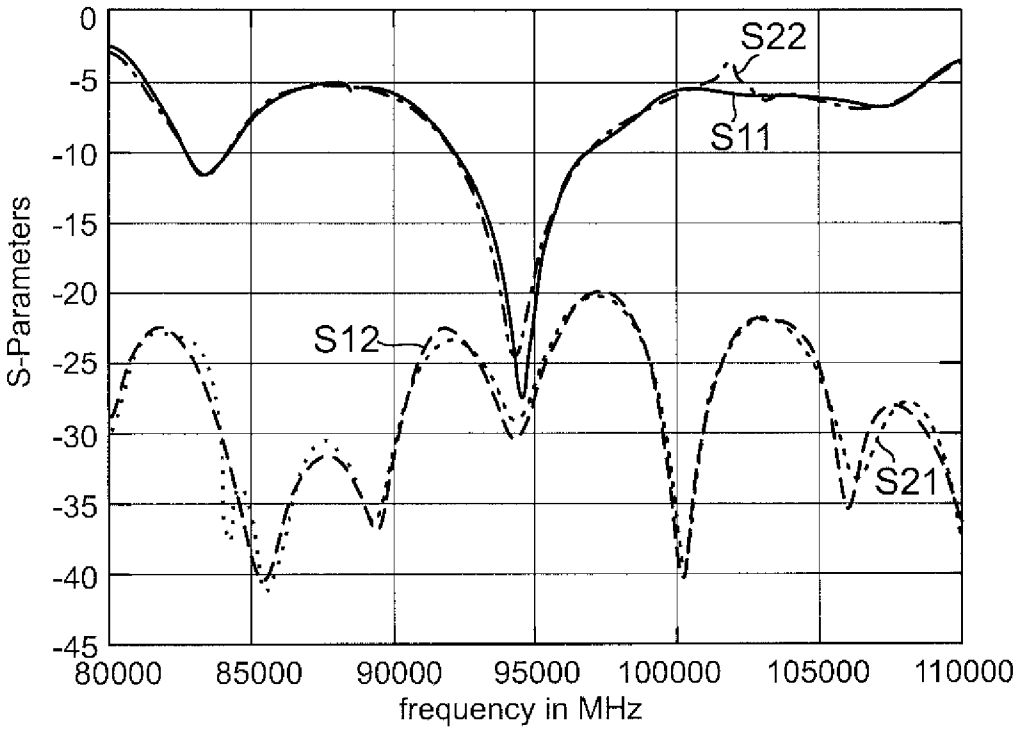

FIG. 15A

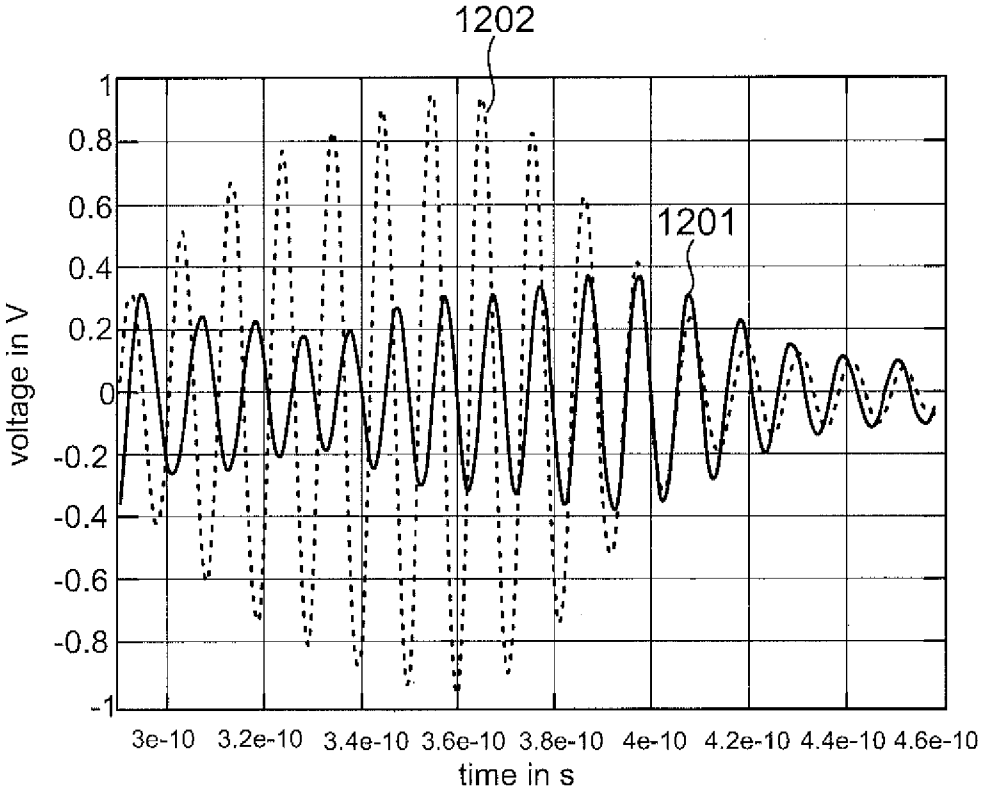

FIG. 15B

WAFER SCALE SENSOR ULTRA-WIDEBAND ARRAY FOR TISSUE DIAGNOSIS

BACKGROUND

1. Field of the Invention

The present invention relates generally to radar imaging systems and, more particularly, to ultra wideband radar systems integrated with wafer scale antenna arrays providing radar sensor and imaging for tissue diagnosis in the field of medicine.

2. Related Art

Among alternatives to conventional methods of breast cancer tumor detection such as mammography, microwave radar techniques appear to be one of the most promising as a result of their potential for being a non-ionizing and low-cost method. Recent research has shown that anomalous tissue may have dielectric constant different from normal living tissue so that differences in tissue relevant to medical diagnosis can be detected using microwave radar. Thus, techniques for microwave radar imaging of living organisms may have, in addition to cancer diagnosis, more general applicability for medical diagnosis.

BRIEF DESCRIPTION OF THE DRAWINGS

FIG. **1** is a perspective view of a wafer scale sensor system used for scanning a person's wrist in accordance with an embodiment of the present disclosure.

FIG. **2**A is an elevation view diagram of a panel of antenna arrays for a wafer scale sensor system in accordance with one or more embodiments; FIG. **2**B is a plan view diagram of a panel of antenna arrays for a wafer scale sensor system in accordance with an embodiment; and FIG. **2**C is another plan view diagram of a panel of antenna arrays for a wafer scale sensor system in accordance with an alternative embodiment

FIG. **3**A is a top-level system block diagram for wafer scale sensor system; FIG. **3**B is a system block diagram showing an example of an architecture for the diagram shown in FIG. **3**A; and FIG. **3**C is a circuit block diagram showing an example of an implementation for the diagram shown in FIG. **3**A, in accordance with one or more embodiments.

FIGS. **4**A and **4**B are display images produced by wafer scale sensor system showing a scan of a person's wrist such as seen in FIG. **1**, in accordance with an embodiment.

FIG. **5**A is a diagram of physical test scenario for scanning body tissue; and FIG. **5**B is an example of an image reconstruction display for the scenario shown in FIG. **5**A, in accordance with an embodiment.

FIGS. **6**A and **6**B are examples of image construction displays for various test subjects, in accordance with one or more embodiments.

FIG. **7** is a plan view diagram showing antenna element and feed network layout for a wafer scale antenna array, in accordance with an embodiment.

FIG. **8** is a schematic diagram showing an example of power or low noise amplifier placement for an antenna array, in accordance with an embodiment.

FIGS. **9**A and **9**B are schematic diagrams showing different examples of power amplifier placement in a feed network for an antenna array, in accordance with an embodiment.

FIGS. **10**A and **10**B are plan view diagrams illustrating unit cells of an antenna array for left hand circularly polarized (LHCP) and right hand circularly polarized (RHCP) performance, in accordance with an embodiment.

FIG. **11** is a graph illustrating insertion loss vs. frequency for a 16-by-16 LHCP antenna array, such as that shown in FIG. **7**, in accordance with an embodiment.

FIGS. **12**A and **12**B are graphs showing co-polarization and cross polarization for wafer scale, LHCP and RHCP antenna arrays, in accordance with an embodiment.

FIG. **13** is a graph showing an example of polarization and enhancement of side lobe suppression for a four-by-four element collimated antenna array, in accordance with an embodiment.

FIG. **14**A is a diagram showing a cross section of a collimator for an antenna array, in accordance with an embodiment; and FIG. **14**B is a perspective diagram of a collimator and a pair of four-by-four element collimated antenna arrays, in accordance with an embodiment.

FIGS. **15**A and **15**B are graphs illustrating an example of cross-coupling and cross-polarization for a pair of four-by-four element antenna arrays, in accordance with an embodiment.

Embodiments of the present disclosure and their advantages are best understood by referring to the detailed description that follows. It should be appreciated that like reference numerals are used to identify like elements illustrated in one or more of the figures, in which the showings therein are for purposes of illustrating the embodiments and not for purposes of limiting them.

DETAILED DESCRIPTION

Methods and systems are disclosed for microwave radar imaging for medical diagnosis that address the need for non-ionizing and low-cost alternatives to conventional medical diagnosis methods. One or more embodiments, for example, may provide non-ionizing alternative to conventional mammography x-ray techniques, which expose patients to ionizing radiation, for breast cancer tumor detection. One or more embodiments, employ a version of an ultra wide band (UWB) sensor that can produce very fine beams at the V- or W-bands by using beam forming techniques developed specifically for wafer scale antenna arrays. Due to the high bandwidth (for UWB, in the range of about 1-10 GHz) of very short pulses at the V-band (e.g., about 40-75 GHz) and W-band (e.g., about 75-110 GHz), radio waves can penetrate tissue and resolve the tissue anomalies with high-resolution. For example, a millimeter-wave radio transmitter emits a train of very narrow pulses. The transiently radiated field impinges on tissues in its field of view and returns a reflected portion of that energy to a correlating receiver. Pseudo-random coding of the pulse train creates a signal and allows the correlating receiver to extract very low energy reflected signals from background noise (e.g., coding gain).

An innovative development uses a highly integrated array of sensor clusters (e.g., panel **200** of antenna arrays **300**) for rapid scan of the subject area, such as breast tissue, to detect anomalies. The integrated array of sensor clusters can eliminate need for mechanical scanning (e.g., moving the sensors relative to the subject) because the wafer scale antenna based array can instantaneously take the desired topographic picture of the subject area, such as breast tissue, and present it in a high resolution display unit or transmit the image data and information wirelessly to a receiver unit. By way of contrast, in a typical synthetic aperture radar (SAR) imaging method, the radio moves along the target (or rotates around it) and scans the surface with a controlled beam width. However, a stationary and electronically steerable array antenna can scan the target with narrow beam width and at much higher speed. As an example a set of radio transceivers would suffice to

achieve a precision detection and location (e.g., range and angle for two-dimensional (2-D)) capability. In order to construct and enhance a SAR type image, the solution of the Helmholtz differential equations for far field (generally distances>10×the wavelength) has been used. Generating a 3-D view of the target requires multiple transceiver arrays or multiple slices of 2-D images generated by application of electronic or mechanical surface scanning of the target. Multiple 2-D views can be captured by the antenna array and computationally merged using processing techniques like diffraction tomography.

Various embodiments may incorporate teachings from U.S. Patent Publication No. 2012/0001674 published Jan. 5, 2012, entitled "Wafer Scale Spatial Power Combiner", and U.S. Patent Publication No. 2013/0307716 published Nov. 21, 2013, entitled "Integrated Ultra Wideband, Wafer Scale, RHCP-LHCP Arrays", which are both incorporated by reference.

FIG. **1** is a perspective view of a wafer scale sensor system **100** used for scanning subject **105** of interest—in this example, a person's wrist—in accordance with an embodiment. FIG. **1** illustrates the position of the subject **105** wrist—having a cyst **106** of approximately 1 centimeter (cm) diameter—with respect to the panel **200** of antenna arrays **300**. As indicated schematically in FIG. **1**, panel **200** of antenna arrays **300** may transmit (TX) and receive (RX) radar signals using beam forming and power combining to produce, for example, narrow radio frequency (RF) pulses at a specific pulse repetition frequency (PRF) in the form of rapid wideband (narrow width) radar pulses at a chosen pulse repetition frequency (PRF) in the 1-10 GHz band. The pulses can penetrate different types of biological tissue with varying attenuation constant. The radar system **100** may, for example, transmit Gaussian pulses as short as a few pico-seconds wide with center frequency in the 1-10 GHz band, FIGS. **4**A and **4**B show examples of images that may be constructed by system **100** for the subject **105** wrist and cyst **106** at 60 GHz (e.g., V-band). Higher frequencies (e.g., 95 GHz, W-band) can produce even finer resolution images.

The electro-magnetic properties of materials, in particular the dielectric properties, e.g., relative permittivity ($\in_r$), exhibit a generally significant contrast in measured value between normal and malignant tissues. Permittivity, being dependent on the frequency of the electric field applied to the material, is usually expressed as a complex number. In general, the permittivity of tumors is much higher than normal tissue, hence, creates the capability to detect pronounced reflections with UWB RF interrogation such as that shown schematically in FIG. **1**. In research and testing scenarios, measurements of relative permittivity of 10−j9 (conductivity of σ=0.4 S/m) for samples of human skin and relative permittivity of 50 (conductivity of σ=4.0 S/m) for malignant breast tissue have been reported. System **100** can exploit complex permittivity characterizations of healthy and malignant tissue for constructing diagnostic images of healthy and malignant tissue.

By measuring the path delay between transmitting and receiving antennas of panel **200** via any desired point in the tissue (e.g., subject **105**), it is then possible to extract and time-align all the signals from that point. Repeated for all points in the tissue hundreds of times, the computational result yields an image in which the distinct dielectric properties of malignant tissue may then be presented. To minimize the clutter arising from the air-tissue interface, undesired reflections may be removed by cancelling out the systematic errors.

Simulation and imaging reconstruction of a single tumor, such as in breast tissue, can be modeled using system **100**, performing simulations and measuring results of tests using malignant tissue detection with a panel **200** of arrays **300** of right-hand and left-hand circularly polarized (RHCP-LHCP) at 60 GHz ultra-wideband (UWB) antennas, using scanning impulses with picoseconds (ps) pulse width as a source, and measuring the reflected waves from the discontinuous layers of dielectric constant (permittivity differences). Since the transmitted pulse may be distorted due to the limiting bandwidth of antennas, it may be necessary to use wideband and non-dispersive antennas for the measurement.

FIG. **2**A illustrates a panel **200** of antenna arrays **300** for a wafer scale sensor system **100** in accordance with one or more embodiments. In order to provide a cost effective, highly reliable, easily portable sensor system **100** with a small footprint, that is easy-to-operate, and is deployable in doctors' offices, health clinics, and hospitals, a highly compact scanning system **100** may be highly desirable, and thus may be implemented using wafer scale antenna arrays **300**. FIG. **2**A illustrates an embodiment of a panel **200** of 24×16 arrays **300** for the scanner of sensor system **100**. In this arrangement 24 columns of TX-RX sensors with their antenna arrays **300** at the V- or W-band may be integrated. If, on one hand, the TX-RX sensors are implemented using one antenna array (not a separate pair of RHCP-LHCP array), then 16 rows of arrays **300** can be addressed for enhanced resolution. On the other hand, if the TX-RX sensors are implemented using pairs of TX-RX with polarization capability (e.g., a separate pair of RHCP-LHCP arrays **300***a*, **300***b*), then 8 rows of arrays **300** can be addressed. In the latter implementation, the advantage of RHCP-LHCP polarization may be an enhanced edge detection at the expense, however, of reduced resolution of image horizontally or vertically depending on orientation of panel **200**.

Similar to the way in which RHCP-LHCP polarization may enhance edge detection of the tumor, use of a linear (e.g., 1×n) array for panel **200** may enhance resolution of the cross section of a tumor that has been detected and imaged. Furthermore, information from reflected signals analyzed by RHCP-LHCP polarization schemes may provide phase information that is also significant to identify the tissue classification, e.g., to detect anomalies.

Furthermore, panel **200** can be vertically flat or curved as shown, respectively, in FIG. **2**B and FIG. **2**C to address imaging relative to subject **105**. The flat panel **200**, as seen in FIG. **2**B, may take less space and be easier to carry, while the radial panel **200**, as seen in FIG. **2**C, of sensor arrays **300** may reduce the load on imaging signal processing. Naturally, other arrangements of the array panel **200** can be pursued depending on the desired applications; for example, a double panel configuration of panel **200** may be used for internal body scanning.

FIG. **3**A illustrates top-level distribution of system functionality, to address considerations relevant to hardware and software layers, for a wafer scale sensor system **100**, in accordance with one or more embodiments.

Considerations at the level of panel **200** of wafer scale antenna arrays **300** may include: footprint of arrays **300** at V- or W-band and physical placement of the antenna arrays **300** and RF arrays **400** relative to each other; physical implementation using flip chip vs. using a single multi-layer board; physical placement of panel **200** on a scanner arm (not shown); and isolation of antenna elements **310** (see, e.g., FIG. **7**) from the RF feeds (TX-RX) **302** (see, e.g., FIG. **7**) with minimal insertion loss.

Considerations at the level of RF arrays **400** (e.g., up and down converters) may include: footprint of arrays **400** at V- or W-band and physical placement of the RF arrays **400** relative to panel **200**; power distribution; phase lock loop (PLL) tuning; physical placement of RF arrays **400** on the scanner arm; and self calibration, RF diagnostics, and test flash.

Considerations at the level of intermediate frequency (IF) arrays **500** (e.g., 3-6 GHz UWB radar) may include: footprint of low power UWB array of signal processor chips (see, e.g., FIG. **3**C); power distribution and power sharing with the RF arrays **400**; PLL tuning hand-shake with the RF arrays **400**; physical placement on the scanner arm; buffering, mux-demux of the Serial Peripheral Interface (SPI) or Universal Serial Bus (USB) based streamed data; upload and download capability of the registers, configuration files, and synchronization with the scanner arm; self calibration, diagnostic, and IF test flash for each channel; power distribution and power sharing with the IF array **500** and RF arrays **400**; and physical placement on the scanner arm.

Considerations at the level of signal management board **600** (e.g., high-end processor board **130** shown in FIG. **3**C) may include: buffering, mux-demux of the SPI or USB based streamed data; upload and download capability of the registers, configuration files, and synchronization with the scanner arm; interface with Windows OS (operating system) and Matlab® based parallel image processing (quad processor) and networking (e.g., network **126** also shown in FIG. **3**C) capability to the operator as well as supervisory level locally and through the "cloud".

FIG. **3**B is a system block diagram showing an example of a particular architecture for the diagram shown in FIG. **3**A. FIG. **3**B shows signal management board **600**, IF arrays (e.g., 3-6 GHz UWB radar) **500**, and RF arrays **400**. Although not shown for clarity in FIG. **3**B, each RF array **400** may be connected to a corresponding TX-RX transceiver **1000** and antenna array **300** as shown in FIG. **3**C.

In one embodiment, for each of the three groups of eight arrays **500**, **400** one of the transceivers may be used as a transmitter and all eight may be used as receivers. The transmitted pulse may be, for example, a first order Gaussian pulse with a center frequency of 4.35 GHz and a bandwidth greater than 2.5 GHz. The receivers may use a sampling on a continuous time binary value to achieve a sampling rate of 40 giga-samples per second (GS/s). Multiple number of the boards can be integrated to address the desired V-band or W-band multiple of 1×8 channels stacked for rapid millimeter wave scan of the tissue (subject **105**) as shown in FIG. **3**B.

In one embodiment using 8 radar chips, timing control may be implemented using field programmable gate array (FPGA) and SPI or USB concatenations for scanning and image construction. By proper processing of the phase shifting in the FPGA, beam steering function can be addressed as well. In such a sequence, as an example, a first transmitter only will trigger and all receiver channels will receive and then a second transmitter only will transmit, and so on. By proper phase management in the digital signal processor (DSP), the arrival time of the wave can be adjusted such that beam steering function is performed.

FIG. **3**C is a circuit block diagram showing an example of an implementation for the diagram shown in FIG. **3**A, in accordance with one or more embodiments. Scanning system **100** may include a number, N, of radar transceivers, such as radar transceiver **1000** illustrated in FIG. **3**C. N may be any number. For example, N may be 24×6=384 radar transceivers **1000** for the embodiment described in FIG. **2**A, or N may be 24 for the embodiment described in FIG. **3**B. System **100** may use an array of transceivers **1000** in which each transceiver is a single-chip radar transceiver realized in complementary metal oxide semiconductor (CMOS) process that may reduce the cost, weight, and energy consumption of system **100** compared to multi-chip radar transceiver implementations, may provide a set of completely isolated transceivers **1000** for system **100**, may provide modularity of the system, and may facilitate extension of its application to medical diagnostic scanning.

In one or more embodiments, the system **100** may employ a either a linear (e.g., 1×n) or rectangular array (e.g., m×n, panel **200**) including one or more sets of multiple single-chip radar transceivers mounted on single FR4 substrate printed circuit boards. In one embodiment, a multiple number of the single-chip radar transceiver boards may be integrated to implement an N-channel linear array for rapid millimeter-wave scan of the subject **105**. One of the transceivers may be used as a transmitter and all of the multiple (for each board) or N transceivers may be used as receivers. The transmitted pulse may be, for example, a first order Gaussian pulse with a center frequency of 4.35 GHz and a bandwidth greater than 2.5 GHz. The receivers may use a sampling on a continuous time binary value to achieve a sampling rate of 40 giga-samples per second (GS/s).

Each transceiver **1000** may be connected via an Ethernet interface **1022** with a processor **130** that may, for example, perform processing that combines data from all transceivers **1000**—whether in a rectangular array or a linear array that is moved to scan the scanning area defined by panel **200**—to provide an image, such as image **122**, on a display **120**. System **100** may also include a supervisor monitoring system **125** that may communicate with processor **130** via a network **126**, as shown, which may include a private secure network, for example, or the Internet.

In system **100**, an array of independent transceivers **1000** (using UWB radar of primary processing unit **1020** as intermediate frequency (IF) and up- and down-converters of RF module **1010** in RF) may be used for extreme near-field imaging. In FIG. **3**C, an arrangement with an integrated IF (radar) board for each transceiver **1000** may operate at 1-10 GHz bandwidth. Results from a mathematical model of system **100** incorporating the inter-sample delay variations show that process variations are a strong influence on image degradation and a factor that is not easily rectified. In one or more embodiments, the problem of inter-sample delay variations may be addressed by direct calibration of the system **100** using one or more reflectors **103** (also referred to as a calibration target) positioned at known locations in the image.

FIGS. **4**A and **4**B are display images produced by wafer scale sensor system **100** showing a scan of a person's wrist such as seen in FIG. **1**, in accordance with an embodiment. As seen in FIG. **1**, subject **105** (person' wrist) may be scanned at a range of a few inches from panel **200** comprising antenna arrays **300**. FIG. **4**A shows constant power contours for the scan of subject **105** and FIG. **4**B shows a spatial image of the hand tissue and anomaly tissue (e.g., cyst **106**). The image of the hand shown in FIGS. **4**A and **4**B may be constructed using a 20×20 position (e.g., panel **200** with TX-RX sensors implemented using pairs of TX-RX with polarization capability, e.g., a separate pair of RHCP-LHCP arrays **300***a*, **300***b* arranged as 20 rows by 10 columns of array **300** pairs) emulated wafer scale antenna array arrangement taken in one second of exposure, where further signal processing of the image demonstrates existence of major change in relative permittivity, showing the anomalous tissue (e.g., cyst **106**) in contrast to normal tissue (e.g., remainder of person's hand). The transmitted power from IF **500** (e.g., 3-6 GHz UWB radar) was about −13 dBm, the RF **400** (e.g., up and down

converters **1010**) transmitted power was less than 50 mW and the beam widths of the TX-RX antennas (e.g., transceivers **1000** and wafer scale antenna arrays **300**) were about 4 degrees. RF operating frequency was from 57 to 60 GHz.

FIG. **5**A is a diagram of physical test scenario for scanning body tissue; and FIG. **5**B shows a graphical user interface display **120** for wafer scale sensor system **100** with an example of an image reconstruction display for the scenario shown in FIG. **5**A. A series of different shape material with high relative permittivity ($\in_2$) inside a low permittivity ($\in_1$) media were subjected to RF scanning and then the reflection image was constructed using a finite difference time domain (FDTD) simulation tool. A method of correlation of the reflected signal with the known transmitted pulse has the lowest detection error and is selected in the simulations. The antenna may be moved along the x-axis to scan the objects. A snapshot of the simulated scenario with the constructed image of multiple objects has been depicted in FIG. **5**B. A Gaussian pulse of 20 GHz bandwidth centered at 60 GHz may be simulated to interrogate the objects located at 49 cm of the antenna plane. Scan is achieved by 21 scan points 2.5 cm apart. FIG. **5**B illustrates the constructed image of the subject **105** with highly reflective material in air. As described above, a relative permittivity of 10−j9 (conductivity of σ=0.4 S/m) for human wrist skin and relative permittivity of 50 (conductivity of σ=4 S/m) may be typical.

FIGS. **6**A and **6**B are examples of image construction displays for test subjects **105**; FIG. **6**A shows image construction from a Circular Scan of Parallelogram shaped test subject **105**; and FIG. **6**B shows image construction from a Circular Scan of a Pyramid shaped test subject **105**. In this scenario, the radar antenna (e.g., array **300**) circles around and scans the target (e.g., subject **105**) from different angles. This mode of operation gives a 2-D view of the object (e.g., subject **105**). In a more practical scenario, a number of antennas (typically 8-16) may be installed in the radar front-end to interrogate different angles. FIG. **6**A shows the scanned image resulting from circular scanning a parallelogram with 36 scan points at 10° steps. FIG. **6**B shows the scanned image result of circular scanning a highly reflective pyramid.

FIG. **7** is an illustration of a wafer scale antenna array **300** showing antenna element and feed network layout for a 16-by-16 antenna element array **300**, in accordance with an embodiment. Wafer scale antenna array **300** may be used, for example, to identify the phase of an object, in case that the array is used as part of a radar transmitter and receiver. In a fully integrated wafer-scale system, the array may be fed from the center as seen in FIG. **7** showing a central array feed **302**. Wafer scale antenna array **300** may include an H-tree feed network **304**, vias **306**, ground plane shield **308**, and UWB spiral antenna plates **310** as a 16-by-16 wafer-scale LHCP array.

FIG. **8** shows an example of power amplifier or low noise amplifier placement for an antenna array, such as arrays **300**, **300***a*, or **300***b*. FIG. **8** shows a 16-by-16 antenna array **420**, with 16 power amplifiers **422**—which may be implemented in Gallium-Nitride (GaN), for example—feeding 256 antenna elements **414**. In a similar example, the 16-by-16 antenna array **420** may be implemented in Gallium-Arsenide (GaAs) with 64 power amplifiers **422** (placed differently as illustrated by the example of FIGS. **9**A and **9**B) feeding the 256 antenna elements **414**. Array **420** may be referred to as a "tile". The spatial combiner of each tile may be manufactured using an H-tree technique of the planar active array, as seen in FIGS. **7** and **8**. Planar antenna array **420** may be disposed "on top of" another similar array **430** having either the same or orthogonal polarization so that arrays **420** and **430** are layered. Thus, a wafer scale antenna module **450** may include integration of the wafer scale RHCP layer antenna array **430** with another layer of LHCP array **420** on top (or bottom). In one or more embodiments, integrated RHCP and LHCP layers **420**, **430** may operate as a wafer scale antenna module **450** that can transmit through the LHCP array and receive waves in the LHCP array as well as the RHCP array, and, conversely, the integrated RHCP and LHCP layers may perform as a wafer scale antenna module **450** that can transmit through the RHCP array and receive waves in the LHCP array as well as the RHCP array.

FIGS. **9**A and **9**B show an example of power amplifier placement variation for a feed network for an antenna array **300**, which may provide flexibility to adjust for differing power and thermal requirements of various materials (e.g., Si, SiGe, GaN, GaAs, and InP) used to implement array **300**. For example, optimal dispersion of power amplifiers **322** in feed network **304** for feeding antenna elements (e.g., spiral antenna plates **310**) may differ from providing one power (or low noise in the case of a receiving antenna array) amplifier **322** per antenna element, as shown in FIG. **9**A, to providing one power (or low noise in the case of a receiving antenna array) amplifier **322** per several antenna elements, for example, four, as shown in FIG. **9**B.

FIGS. **10**A and **10**B illustrate unit cells **301**, **302** of an antenna array (e.g., wafer scale antenna array **300**) for left hand circularly polarized (LHCP) and right hand circularly polarized (RHCP) performance. The form and dimensions of each spiral plate **310** may be defined or determined using the following equations.

Outer spiral circumference may be defined by Equations (1) and (2):

$$Xo=Ao*d*\mathrm{Cos}(Bo+ba)+\mathrm{off}+Cox \tag{1}$$

$$Yo=Ao*d*\mathrm{Sin}(Bo+ba)+\mathrm{off}+Coy \tag{2}$$

For 95 GHz operation, for example, the following values may be used:

Ao=5 to 101
Bo=0.08 to 1.76
ba=6.2
d=4.5
off=0
Cox=109
Coy=189

Inner spiral circumference may be defined by Equations (3) and (4):

$$Xi=Ai*d1*\mathrm{Cos}(Bi+ba)+\mathrm{off}+Cix \tag{3}$$

$$Yi=Ai*d1*\mathrm{Sin}(Bi+ba)+\mathrm{off}+Ciy \tag{4}$$

For 95 GHz operation, for example, the following values may be used:

Ai=5 to 101
Bi=0.08 to 1.76
ba=6.2
d1=6.0
off=0
Cix=109
Ciy=189

FIG. **11** is a graph illustrating insertion loss vs. frequency for a 16-by-16 LHCP antenna array, such as that shown in FIG. **7**, in accordance with an embodiment. FIG. **11** shows a graph of insertion loss (in dB) vs. frequency (in MHz) using S-parameters (e.g., a mathematical construct that quantifies how RF energy propagates through a multi-port network; for example, S**11** may refer to the ratio of signal that reflects from

port one for a signal incident on port one) for a 16×16 LHCP antenna array (e.g., wafer scale antenna array **300**) which operates around a center frequency of 95 GHz.

FIGS. **12**A and **12**B show co-polarization and cross polarization graphs for wafer scale, LHCP and RHCP antenna arrays (e.g., similar to wafer scale antenna array **300**). FIG. **12**A shows wafer scale beam forming of an LHCP array with left-hand circular polarization (co-polarization) beam **801** and cross polarization **802**. As can be seen from the graph, beam width of better than 4 degrees can be obtained, with a 22 dB gain difference for cross polarization suppression of the RHCP wave **802**. FIG. **12**B shows similar results for wafer scale beam forming of an RHCP array (e.g., similar to wafer scale antenna array **300**) with right-hand circular polarization (co-polarization) beam **803** and cross polarization (LHCP) **804**.

FIG. **13** shows a graph of an example of polarization and enhancement of side lobe suppression for a 4×4 element collimated antenna array. In one embodiment, an "out-of-phase squeezing" of the transmitted waves permits a smaller array to deliver similar gain, beam width, and polarization properties with substantially reduced number of array elements compared to a larger array such as the (256-element) antenna array **300** and may reduce the need for integration of complex power amplifiers with the antenna array, reducing the integration level, power consumption, and cost. In one embodiment, the enhancement using "out-of-phase squeezing" may permit using a 4-by-4 element (16 antenna elements) or 8×8 elements (64 antenna element) array instead of, for example, the implementation of the 16×16 (256 antenna elements) antenna array **300** such as shown in FIG. **7**. Such an antenna size reduction confers the capability to reduce various radar system sizes by a factor of 4 as well as packing alternating right-hand circularly polarized (RHCP) and left-hand circularly polarized (LHCP) 4×4 arrays in a planar surface to provide higher radar image resolution and phase contrast with minimal thickness of the arrays.

In addition, use of a separate wafer scale collimator layer **1100** (see FIG. **14**B) that is separated from the antenna array by a certain distance may be implemented. Such a collimator may be implemented as a 4×4 array of Teflon based (e.g., $\in_r$=2.0, where $\in_r$ is the relative permittivity of the material as opposed to the vacuum permittivity $\in_0$) collimators that produce a beam width of approximately 8.0 degrees and a gain of 24.4 dB with 24 dB cross polarization. The index of refraction (or permittivity) of the collimators can vary among various embodiments.

The graph in FIG. **13** shows co-polarization and cross-polarization of the LHCP radiation and RHCP radiation of the 4×4 array **1102** with Teflon wafer-scale collimator **1100** shown in FIG. **14**B. The size of the 4×4 array **1102** operating at 95 GHz may be about 5.6 mm by 5.6 mm. FIG. **13** shows side lobes are below 3 dB with a better than 20 dB side lobe suppression compared to the 16×16 array **300** that has two strong side lobes at 12 dB. Suppression of side lobes may be a critical factor for clear radar imaging with high contrast and high antenna efficiency (e.g., greater than 95%).

FIG. **14**A is a diagram showing a cross section of a collimator for an antenna array such as shown in FIG. **14**B; and FIG. **14**B is a perspective diagram of a collimator layer and a pair of 4-by-4 element collimated antenna arrays, in accordance with an embodiment. FIG. **14**B depicts the implemented collimator **1100** at the position, relative to array **1102**, of enhancing the gain and reducing side lobes. As shown in FIG. **10**B, one 2×2 LHCP array and one 2×2 RHCP array may be integrated in the same substrate side by side. Spacing between the collimator **1100** and the array plates **1102** may be about 20 mm for a combination of collimator patterns with each protrusion upward and inward with effective radius of 20 mm and total thickness of 5 mm. Four double-sided protrusions may be placed atop of each 2×2 sub-array.

FIGS. **15**A and **15**B are graphs illustrating an example of cross-coupling and cross-polarization for a pair of four-by-four element antenna arrays, in accordance with an embodiment. To verify lack of cross coupling, the S**11**, S**12**, S**22**, and S**21** S-parameters, as shown in FIG. **15**A, were measured.

FIG. **15**B shows a graph of voltage **1201** cross coupled during transmission and then returned, in response to a modulated UWB Gaussian pulse **1202**, from a metallic reflector placed 53 mm away from the (co-polarized) array **1102** for simulation purposes, illustrating that the returned voltage **1201** from the metallic reflector is highly detected by the cross-polarized array **1102**.

Such simulation results, summarized in Table 1, may show, for example, that a 4×4 element array may have nearly the same gain, superior side lobe suppression, and enhanced cross polarization suppression, while its size is about 25% of an 8×8 array and 6% of a 16×16 array.

TABLE 1

	System	
	16 × 16	4 × 4 with Collimator
Center Frequency (GHz)	95	95
Badwidth (GHz)	4	4
Beamwidth (o)	4	8
Antenna Gain (dB)	26	24
Sidelobe (dB)	13	3
Cross-Polarization Supression (dB)	22	24
Dimensions (L mm × W mm)	22.4 × 22.4	5.6 × 5.6

Embodiments described herein illustrate but do not limit the disclosure. It should also be understood that numerous modifications and variations are possible in accordance with the principles of the present disclosure. Accordingly, the scope of the disclosure is best defined only by the following claims.

What is claimed is:

1. A system comprising:

a panel of planar antenna arrays, each planer antenna array comprising a plurality of circularly polarized antenna elements in a planar surface, wherein each antenna element includes a spiral plate;

an array of converters for converting an ultra wide band (UWB) radar signal to V-band or W-band frequency;

a feed network connecting the V-band or W-band frequency signal to each of the antenna elements; and

a plurality of amplifiers dispersed in the feed network and configured to provide spatial power combining and beam forming of the V-band or W-band frequency signal for high resolution detection of a tissue anomaly.

2. The system of claim **1**, further comprising a signal processor that is configured to:

measure a path delay between a transmitting antenna and a receiving antenna of the panel via a point in the tissue;

extract and time-align the spatially beam formed signal from the point; and

perform image processing using the extracted and time-aligned signal to provide an image presenting the distinct dielectric properties of the tissue anomaly.

3. The system of claim **1**, wherein:

the signal includes a transmitted signal and the amplifiers comprise power amplifiers.

4. The system of claim 1, wherein:
the signal includes a received signal and the amplifiers comprise low noise amplifiers.

5. The system of claim 1, wherein the system includes:
an image processor that combines processing from both right hand circularly polarized (RHCP) reflected signals and left hand circularly polarized (LHCP) reflected signals to provide enhanced edge detection of the tissue anomaly.

6. The system of claim 1, wherein the system includes:
an image processor that analyzes information from both right hand circularly polarized (RHCP) reflected signals and left hand circularly polarized (LHCP) reflected signals to provide phase information for detection of the tissue anomaly.

7. The system of claim 1, wherein:
the signal comprises a pseudo-random coding that allows a correlating receiver to extract very low energy reflected signals from background noise to provide a coding gain.

8. The system of claim 1, wherein:
the panel of planar antenna arrays comprises a linear, 1×n, array to provide enhanced resolution of the cross section of the tissue anomaly.

9. A method for detecting a tissue anomaly in a subject, comprising:
scanning the subject using a spatially beam formed, high resolution radio frequency signal transmitted from a panel of antenna arrays;
measuring a path delay between a transmitting antenna and a receiving antenna of the panel via a point in the tissue anomaly;
extracting and time-aligning the spatially beam formed radio frequency signal from the point; and
performing image processing using the extracted and time-aligned signal to provide an image presenting the distinct dielectric properties of the tissue anomaly.

10. The method of claim 9, wherein scanning further comprises:
transmitting from a first transceiver in an array comprising a plurality of transceivers; and
receiving from all receivers in the plurality of transceivers of the array.

11. The method of claim 9, further comprising:
performing the scanning in a single exposure without mechanical movement of the panel relative to the subject during the scanning.

12. The method of claim 9, further comprising:
performing spatial power combining and beam forming of the transmitted signals via a plurality of power amplifiers dispersed in the feed network.

13. The method of claim 9, further comprising:
performing spatial power combining and beam forming of the received signals via a plurality of low noise amplifiers dispersed in the feed network.

14. The method of claim 9, further comprising:
scanning using the spatially beam formed radio frequency signal comprising an ultra wide band (UWB) pulse for detecting differences in permittivity of the subject and the tissue anomaly.

15. The method of claim 9, further comprising:
performing spatial power combining and beam forming from an antenna array comprising alternating right-hand circularly polarized (RHCP) and left-hand circularly polarized (LHCP) for enhanced edge detection of the tissue anomaly.

16. The method of claim 9, further comprising:
analyzing information from both right hand circularly polarized (RHCP) reflected signals and left hand circularly polarized (LHCP) reflected signals to provide phase information for detection of the tissue anomaly.

17. The method of claim 9, wherein:
the panel of antenna arrays comprises a linear, 1×n, array to provide enhanced resolution of the cross section of the tissue anomaly.

18. The method of claim 9, wherein scanning comprises transmitting and receiving the radio frequency signal in the V-band or the W-band for enhanced resolution of the tissue anomaly.

19. The method of claim 9, wherein:
the signal comprises a pseudo-random coding that allows a correlating receiver to extract very low energy reflected signals from background noise to provide a coding gain.

* * * * *

UNITED STATES PATENT AND TRADEMARK OFFICE

CERTIFICATE OF CORRECTION

PATENT NO.	: 9,372,256 B2
APPLICATION NO.	: 14/191118
DATED	: June 21, 2016
INVENTOR(S)	: Farrokh Mohamadi

It is certified that error appears in the above-identified patent and that said Letters Patent is hereby corrected as shown below:

In the specification

In Column 5, Line 64, change "6" to --16--.

In Column 10, Line 29, change "Badwidth" to --Bandwidth--.

In Column 10, Line 33, change "Supression" to --Suppression--.

Signed and Sealed this
Twenty-third Day of August, 2016

Michelle K. Lee

Michelle K. Lee
Director of the United States Patent and Trademark Office